Proc. SPIE, 310: 143-150, 1981

Particulate model for halftone noise in electrophotography II. Experimental verification

R. Shaw, P. D. Burns
Xerox Corporation, Webster, New York 14580
J. C. Dainty
Institute of Optics, University of Rochester, New York 14627

Abstract

The various measurements necessary to test the model constructed in Part I of this paper are described. These measurements are used to calculate the model constituents of electrophotographic halftone noise, and hence to predict the overall noise. The predictions are then themselves compared with practical measurements of overall noise, and a close fit is found between theory and experiment. The fundamental role of toner particle size is confirmed.

Introduction

In Part I of this paper we developed a model for the overall noise associated with halftone dots formed by aggregations of toner particles. To verify this model it is necessary to compare experimental results with model predictions, which themselves require experimental measurements of the appropriate statistical dot properties. Here we shall initially concern ourselves with the measurements of the dot properties as they influence the constituents of the noise model. We shall then use these constituents to predict the overall noise.

For the practical measurements we chose a laboratory image typical of electrophotographic halftones. Two halftone frequencies were selected (nominally 65 and 120 per inch), and step tablet inputs were used to obtain uniform image density levels for both frequencies. The input document also contained a solid-area step tablet to enable the solid-area Wiener Spectrum values to be incorporated in the halftone model. Although the halftone step tablets on the input document contained fractional dots in the 5 to 95% range, our measurements were made only on dots in the 5 to 50% range, since as discussed in Part I our model assumptions are probably only realistic in this region. A later paper will discuss the higher density region, which also involves additional measurement problems not addressed here.

Measured Dot Properties

Our model calculations indicated the primary role of the fluctuations in dot size in determining the overall halftone noise. Thus we start here by investigating the validity of our assumptions relating to this component.

Dot area measurements were made using a Quantinet image analyzer. This instrument, equipped with a TV type camera, samples the object with several thousand picture elements (pixels typically 1.8 x 1.8 μm). The measurement of geometrical dot area is obtained by counting the fraction of pixels whose signal exceeds a threshold (nominally close to background level). The frame size is adjusted to that of a single halftone cell. A series of cells are measured to yield both the mean and mean-square fluctuation (A_1 and $\sigma_{A_1}^2$) of the halftone dot area. The mean area was calculated from thirty separate dot measurements. The measurements are shown in summary form in Table I.

To test the validity of equation (14) of Part I, the mean-square fluctuation in dot area was plotted as a function of the mean area, as shown in Fig. 1. Results for both screen frequencies are shown on the same plot, since the assumptions of equation (14) are that the area fluctuations depend only on absolute dot area and hence are independent of halftone frequency (identical areas at different halftone frequencies will of course correspond to different fractional area coverages).

Figure 1 demonstrates the linear relationship between the mean and mean-square fluctuation as predicted by the model, with the two separate frequency populations falling within a single overall population. From these experimental results we can use equation (14) to deduce the area of the individual particles forming the dots, determined simply as the slope of Fig. 1. A least-square linear fit to the data of Fig. 1, plus the assumption of circular toner particles, leads to calculated geometrical cross-section area of 256 μm^2, or a diameter of 18.1 μm. Separate measurements taken on fused toner particles within

Nominal 65/inch Halftone Cell Size 389 x 389 μm				Nominal 120/inch Halftone Cell Size 211 x 211 μm			
d_1 μm	f_1	A_1 $\mu m^2 x10^{-4}$	$\sigma_{A_1}^2$ $\mu m^2 x10^{-6}$	d_1 μm	f_1	A_1 $\mu m^2 x10^{-4}$	$\sigma_{A_1}^2$ $\mu m^2 x10^{-6}$
156	.126	1.91	5.3	63	.065	0.31	2.6
182	.173	2.61	12.5	87	.126	0.59	3.3
235	.286	4.33	8.9	115	.221	1.03	2.5
271	.383	5.79	11.1	138	.318	1.49	5.9
292	.441	6.67	13.1	156	.410	1.92	7.6
316	.519	7.85	20.6	170	.484	2.26	5.1

Table I. Measured values of halftone dot area and the mean square fluctuation in area.

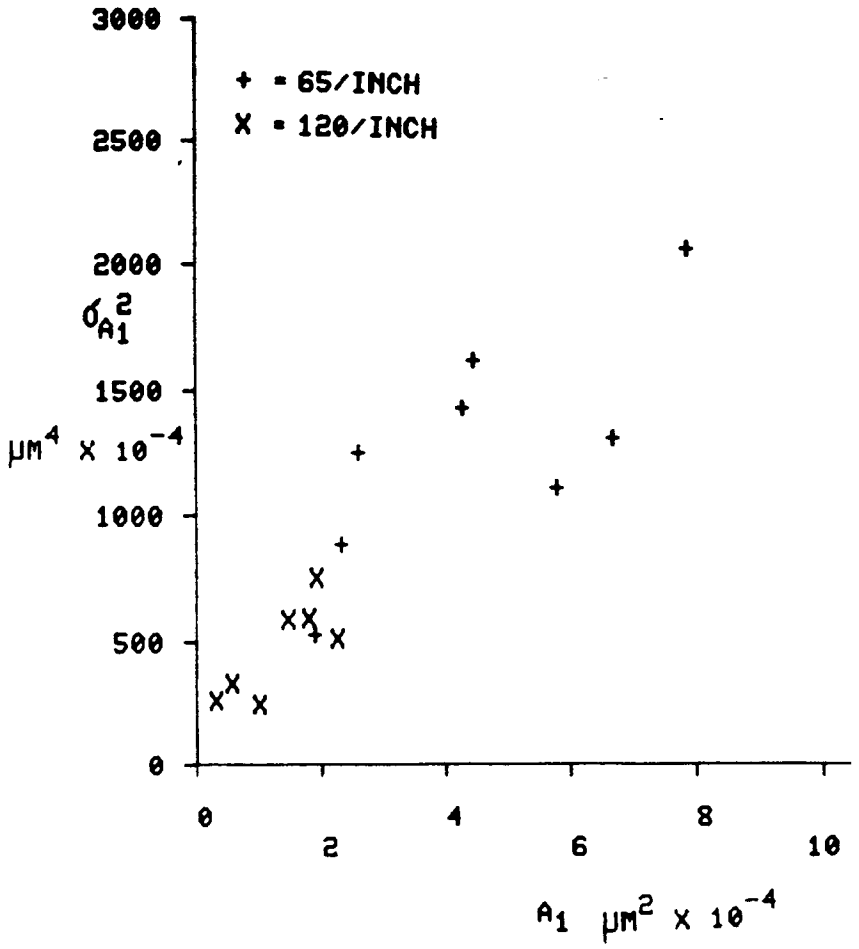

Figure 1. Measured dot area variance versus average area.

background areas indicate a mean diameter of approximately 16.5 μm. From this close fit between theory and result, we can, by the nature of the theory in Part I, deduce that the dot area fluctuation is indeed determined by the underlying statistics governing the fluctuations in numbers of toner particles from dot to dot. In this sense the noise level is probably down to a fundamental level governed by the constituent toner particles. Halftone images formed with smaller toner particles would imply smaller fluctuations in dot area, and this hypothesis will be investigated in future work.

We can now express the noise associated with the dot-area fluctuations in absolute Wiener Spectrum terms by the use of equation (11). To do this it is also necessary to measure the local reflectances of the dot and surround. Densitometric measurement of dot reflectance was accomplished using a microdensitometer with a square aperture (30 μm x 30 μm for the smallest dot). The average dot reflectance R_1 was calculated from measurements within fifty separate dots. A similar measurement was made for the reflectance of background. The results are summarized in Table II.

65/inch Halftone				120/inch Halftone			
f_1	R_1	f_2	R_2	f_1	R_1	f_2	R_2
0.126	0.115	0.874	0.794	0.065	0.309	0.935	0.794
0.173	0.079	0.827	0.794	0.126	0.195	0.874	0.794
0.286	0.069	0.714	0.794	0.221	0.129	0.779	0.794
0.383	0.058	0.617	0.794	0.318	0.123	0.682	0.794
0.441	0.055	0.559	0.794	0.410	0.087	0.590	0.794
0.519	0.058	0.481	0.794	0.484	0.079	0.516	0.794

Table II. Measured values of reflectance within-dot and background.

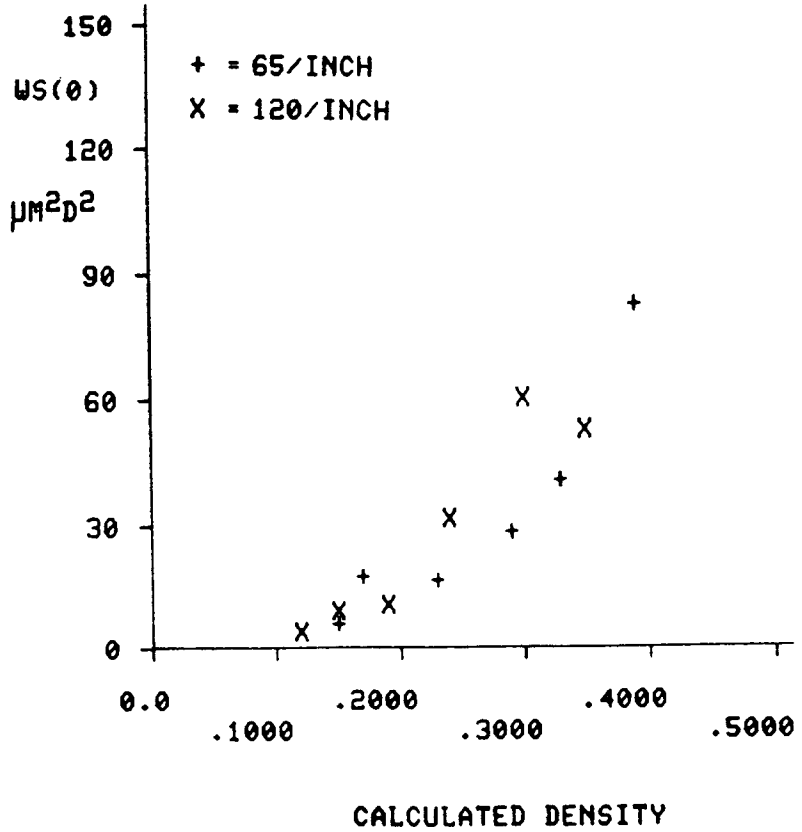

Figure 2. Calculated noise due to dot-area fluctuation.

We list the reflectances of background (R_2), although this value is of course constant throughout. The within-dot reflectance varies somewhat as a function of dot size, especially at low dot sizes where the central region of the dot does not reach saturation density. For larger dots the reflectance becomes approximately invariant with dot-size, corresponding to saturation density (in this case at a density of around 1.25).

Predicted Noise Due to Dot-Area Fluctuations

We have now established the parameters necessary for calculating the noise due to dot-area fluctuations via equation (11). This is shown plotted in Fig. 2, where the Wiener Spectrum levels for both halftone frequencies are shown as a function of the mean density, calculated via equation (2). We again note that, in these terms, the two frequencies form a single population.

At this stage we must consider an important practical aspect of image density, related to the paper substrate, namely the well-known Yule-Nielsen effect[1]. Due to the spread function associated with the substrate the dimensions of the image-forming units (particles or dots) which contribute to image density are not identical to the geometrical properties we have used throughout in our model derivation. In this present context we note merely that when the paper spread function is large compared to particle diameter, the effective cross-section area of a particle of area A_1 is simply $2A_1$. For larger particles or dots the factor will be less than two, since in effect not all the underside of the particle will then have incident (scattered) light to absorb.

Calculations for the present practical images showed that only the larger dots of the coarse (65/inch) halftone would have a Yule-Nielsen factor slightly less than two. This is illustrated in Fig. 3, which shows the Yule-Nielsen factor as a function of dot area, as calculated for the substrate of the experimental images. To correct for this essential factor we have to replace A_1 in the hitherto purely geometric model with the appropriate factor deduced from Fig. 3 for each specific dot area.

We show the noise values corrected by these appropriate values, in Fig. 4. At this stage we introduce the measured mean density level rather then the model (geometric) density of equation (2). The measured density of course automatically includes the appropriate Yule-Nielsen effect, and it is not the purpose of this present paper to verify our model for the mean density level of electrophotographic halftones. We will report separately on this.

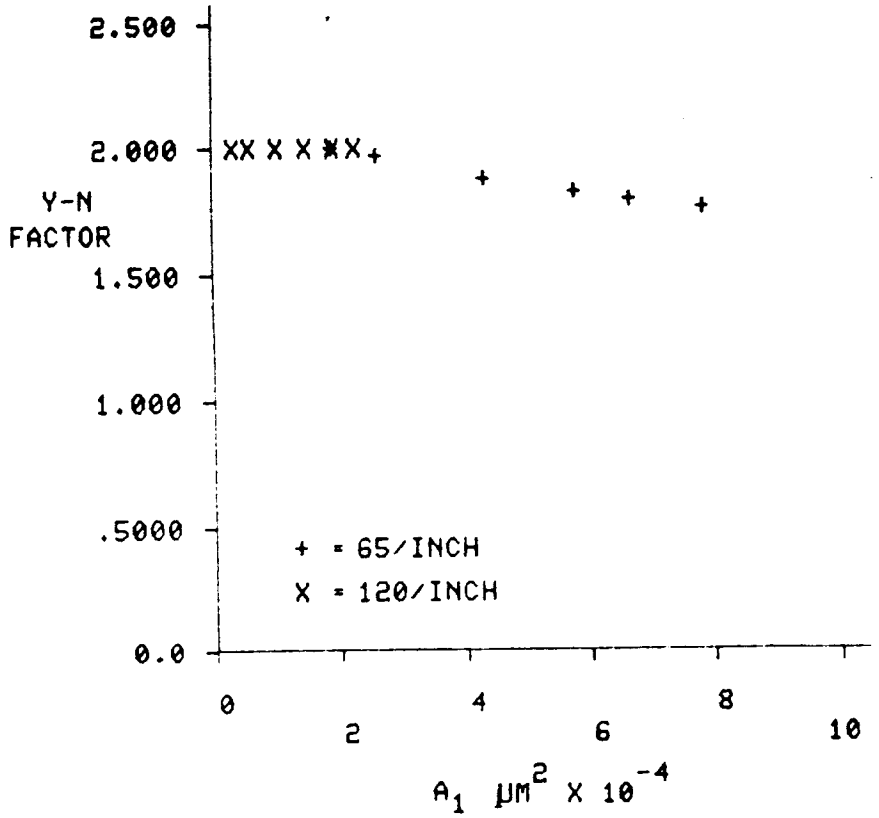

Figure 3.
Yule-Nielsen factor versus dot area.

Before comparing the results of Fig. 4 with the measured overall noise, it is necessary to add the model component due to within-dot fluctuations, although we already know that this component is small.

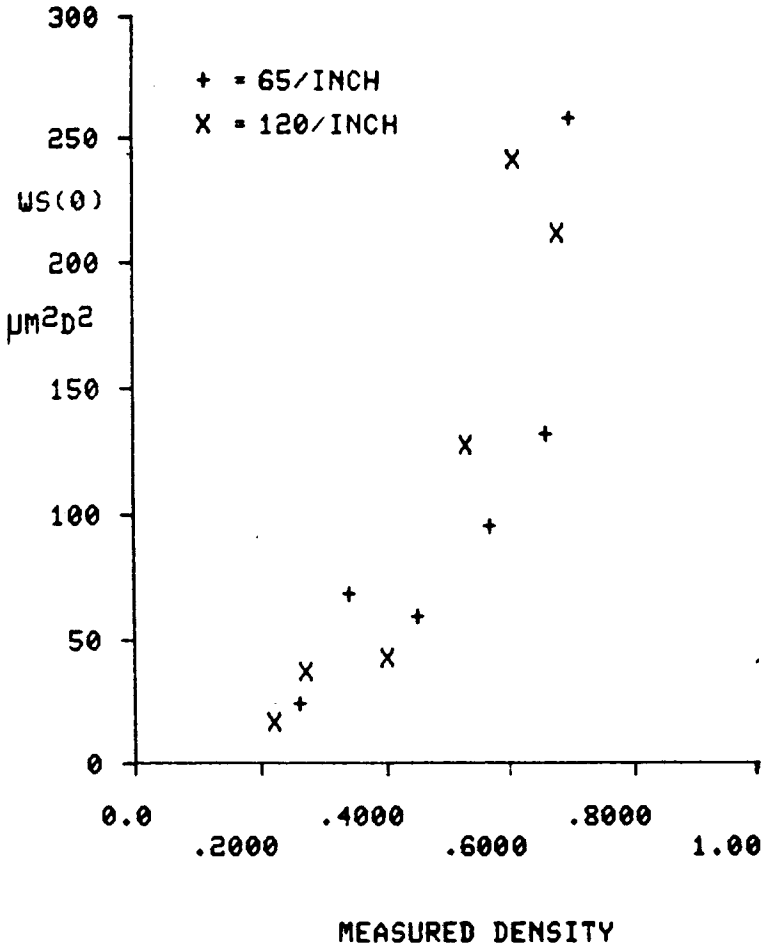

Figure 4. Model dot area noise calculation, including the Yule-Nielsen factor, versus measured cell density.

Predicted Noise Within-Dot and Background

We obtained the Wiener Spectrum values corresponding to within-dot and background fluctuations from experimental measurements on the image of the accompanying solid area step tablet. We could of course have deduced these values from the model Siedentopf equation for solid areas, based on a particle diameter of 16.5 μm and appropriately corrected for the Yule-Nielsen effect. However, again, we are not concerned here with a model for solid-area noise, hence the experimental measurements.

The measurements shown in Fig. 5 were obtained using an effective 25 μm x 1 mm slit, scanned across the solid area images. A 25 μm sampling interval was used, and 40 blocks of 50 data values were transformed to obtain a Wiener Spectrum estimate[2] with standard error around 16%. The spectrum thus obtained was used to deduce a very low frequency estimate, WS(0).

$WS_1(0)$ and $WS_2(0)$ of equation (6) were read-off from a straight line fit to the data of Fig. (5), at the appropriate (high) dot and (low) background density levels. As a matter of interest, the Siedentopf equation was used to predict the toner particle diameter (again assumed constant) yielding a value of around 35 μm, i.e., somewhat higher than that measured directly.

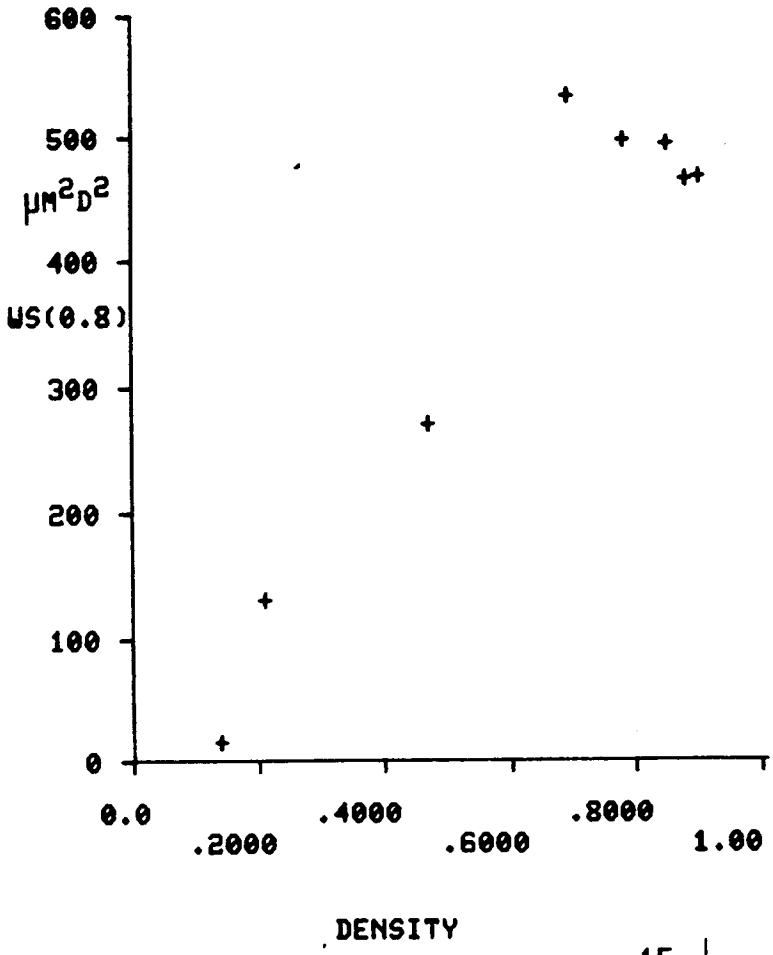

Figure 5. Measured low frequency solid area Wiener Spectrum-density characteristics.

The appropriate values of WS_1 and $WS_2(0)$, combined with the corresponding fractional areas and reflectances of Table II, were used to calculate the two right-hand-side components of equation (6). These components are shown in Figures 6(a) and (b) for the two halftone frequencies. As anticipated, these are significantly less than the noise levels due to dot-area fluctuations.

Predicted Overall Halftone Noise

We now form the overall halftone noise, as predicted by our model by summing the contributions from area fluctuations and within-dot and background fluctuations. The result is shown in Fig. 7, the noise levels of which are of course virtually unchanged from those of Fig. 4.

Measured Overall Halftone Noise

The final set of experimental measures concerns the overall noise associated with halftones. We recall that the halftone noise model results in an overall predicted Wiener Spectrum, estimated by the product of cell area with mean-square density fluctuation as measured from dot-to-dot. This measurement was obtained using a square sampling aperture the size of the halftone cell. The density of

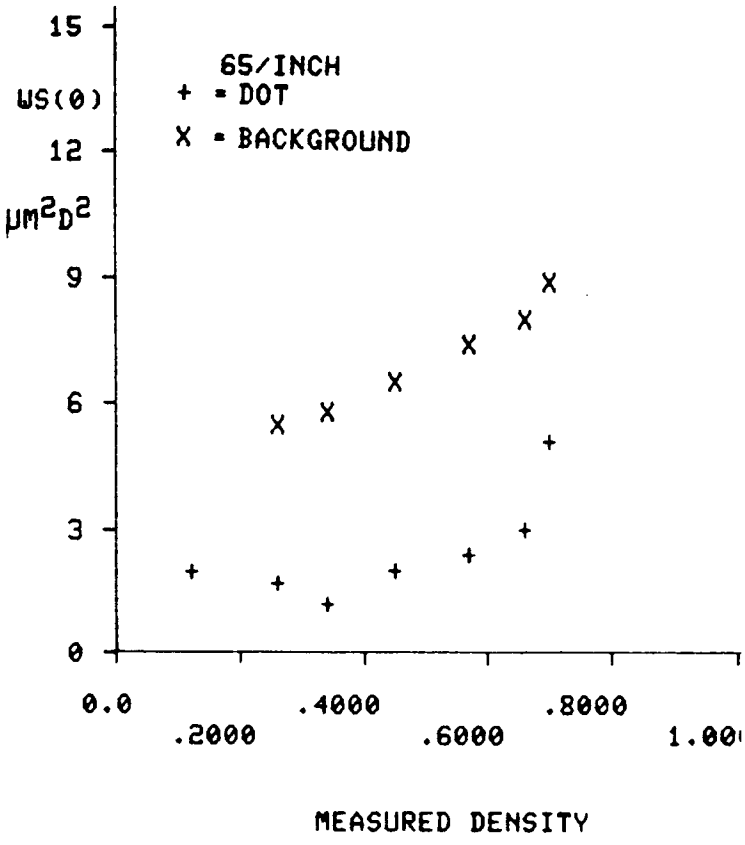

Figure 6(a). Calculated noise due to dot density fluctuation (65 inch halftone).

consecutive cells were measured by moving the aperture one cell side, $\sqrt{A}$, between samples. A data point was recorded when the halftone dot was centered within the aperture. The value $A\sigma^2$ was then calculated from the measurements of sample size 30, and the results are shown in Fig. 8, plotted as a function of measured density level. Figs.7 and 8, thus form the essential sets of data for the comparison of the model predictions with the observed noise.

Comparison of Model and Measurements

Fig. 9 shows the respective curves fitted to the data of Figs. 7 and 8. The close fit both on absolute magnitude and in curve shape is reassuring that, in spite of our various assumptions, approximations and measurement inacurracies, we have captured the essential constituents of electrophotographic halftone noise in our model.

The slight systematic overprediction of the noise level by the model will be the subject of further more detailed experiments.

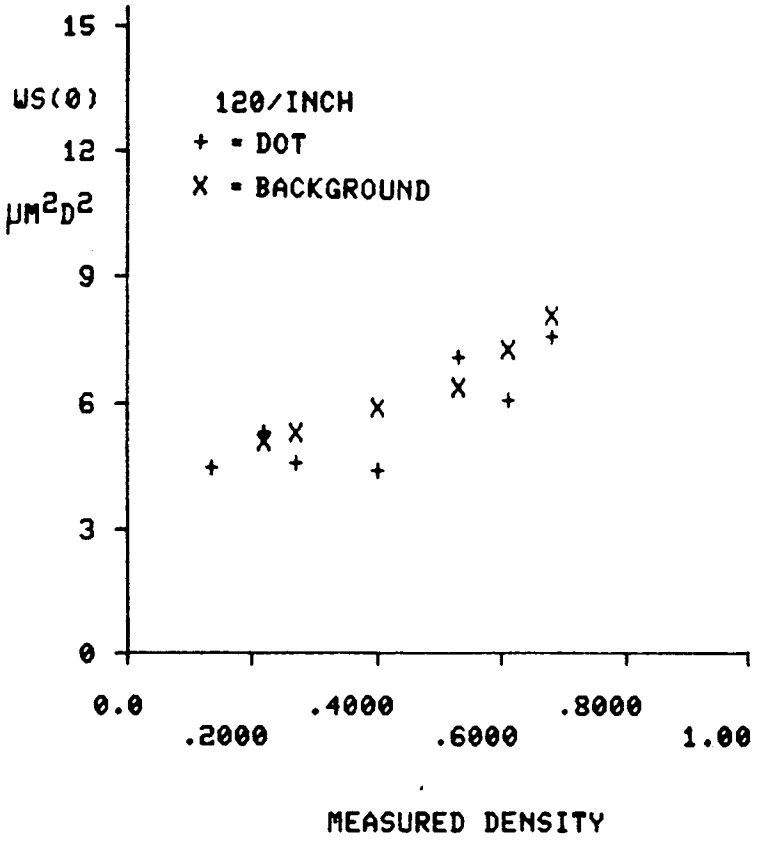

Figure 6(b). Calculated noise due to dot density fluctuation (120/inch halftone).

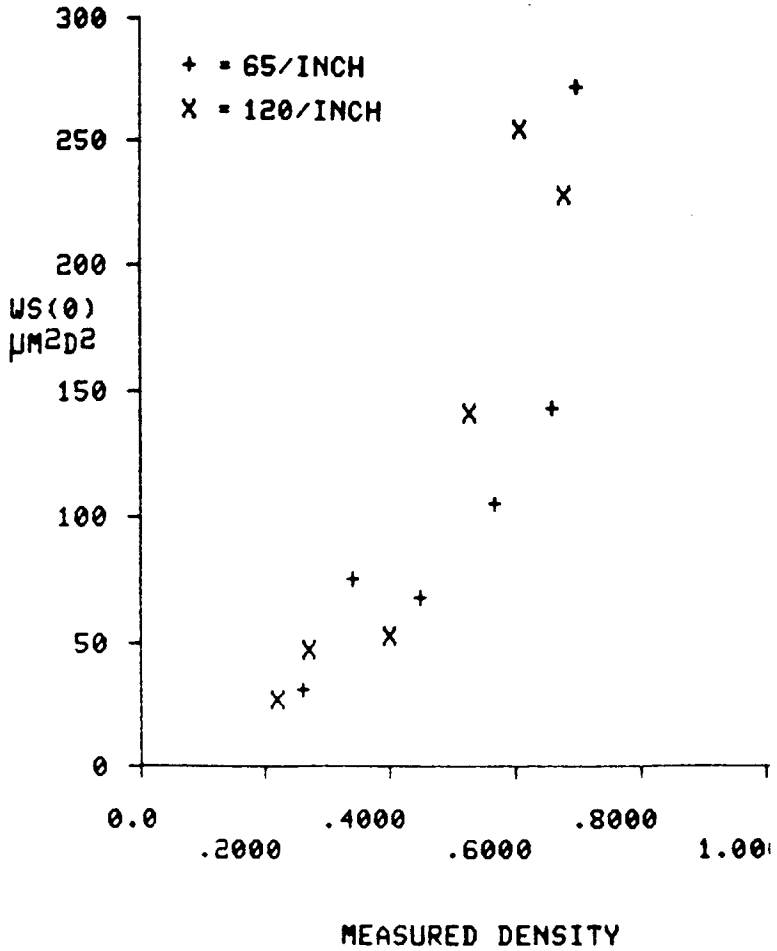

Figure 7. Total halftone noise according to model (including Yule-Nielsen factor) versus measured density.

Conclusion

We have established a model for noise in electrophotographic halftones which has identified the relative roles of the various constituents of the overall noise level. The model provides a satisfactory explanation for the essential difference in shape between the observed noise-density characteristics for solids and halftones.

The dominant role of the fluctuation in dot size has been established, and this in turn related directly to the statistics of the toner particles forming the dot, and especially their size.

Acknowledgement

It is a pleasure to acknowledge the assistance of Terry Kimbrough, who carried out the experimental measurements reported in this paper.

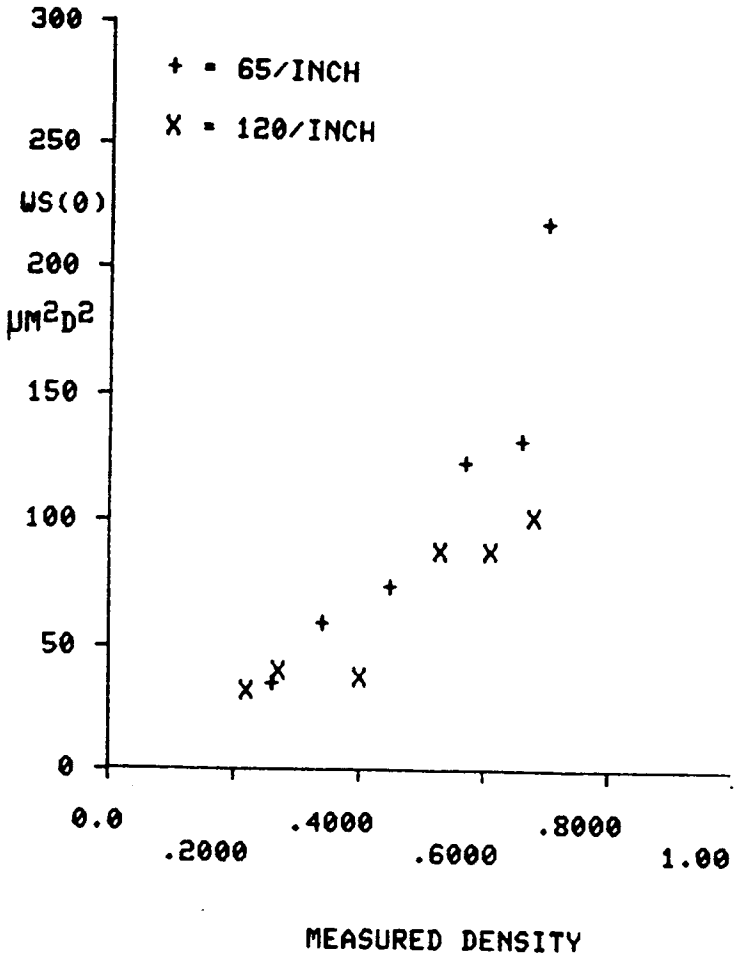

Figure 8. Measured halftone noise ($A\sigma_A^2$) versus density.

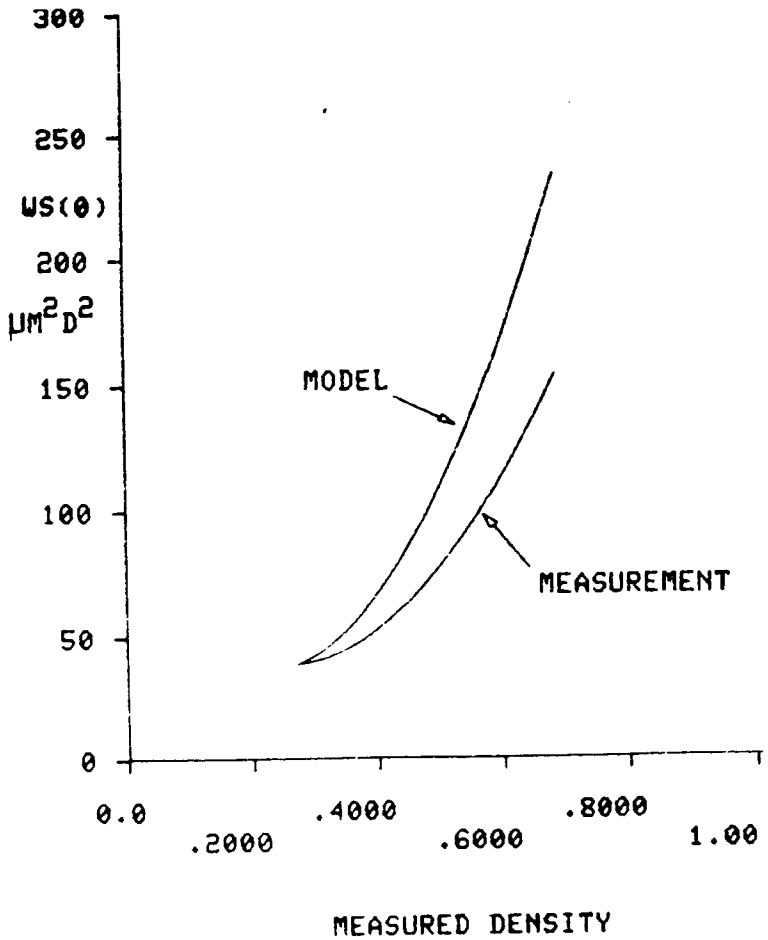

Figure 9. Comparison of halftone noise model and measurement.

References

1. Yule, J.A.C. & Nielsen, W.J., TAGA Proc. 3, p. 65 (1957).
2. Dainty, J.C. & Shaw, R., Image Science, Academic Press, pp. 292-296 1974.